

Communication

Nanoscale Metal-Organic Frameworks Stabilize Bacteriochlorins for Type I and Type II Photodynamic Therapy

Taokun Luo, Kaiyuan Ni, August Culbert, Guangxu Lan,
Zhe Li, Xiaomin Jiang, Michael Kaufmann, and Wenbin Lin

J. Am. Chem. Soc., **Just Accepted Manuscript** • DOI: 10.1021/jacs.0c02129 • Publication Date (Web): 04 Apr 2020

Downloaded from pubs.acs.org on April 4, 2020

Just Accepted

"Just Accepted" manuscripts have been peer-reviewed and accepted for publication. They are posted online prior to technical editing, formatting for publication and author proofing. The American Chemical Society provides "Just Accepted" as a service to the research community to expedite the dissemination of scientific material as soon as possible after acceptance. "Just Accepted" manuscripts appear in full in PDF format accompanied by an HTML abstract. "Just Accepted" manuscripts have been fully peer reviewed, but should not be considered the official version of record. They are citable by the Digital Object Identifier (DOI®). "Just Accepted" is an optional service offered to authors. Therefore, the "Just Accepted" Web site may not include all articles that will be published in the journal. After a manuscript is technically edited and formatted, it will be removed from the "Just Accepted" Web site and published as an ASAP article. Note that technical editing may introduce minor changes to the manuscript text and/or graphics which could affect content, and all legal disclaimers and ethical guidelines that apply to the journal pertain. ACS cannot be held responsible for errors or consequences arising from the use of information contained in these "Just Accepted" manuscripts.

Nanoscale Metal-Organic Frameworks Stabilize Bacteriochlorins for Type I and Type II Photodynamic Therapy

Taokun Luo,^{1,‡} Kaiyuan Ni,^{1,‡} August Culbert,¹ Guangxu Lan,¹ Zhe Li,¹ Xiaomin Jiang,¹ Michael Kaufmann¹ and Wenbin Lin^{1,2,*}

¹Department of Chemistry and ²Department of Radiation and Cellular Oncology and Ludwig Center for Metastasis Research, The University of Chicago, Chicago, IL 60637, USA

Supporting Information Placeholder

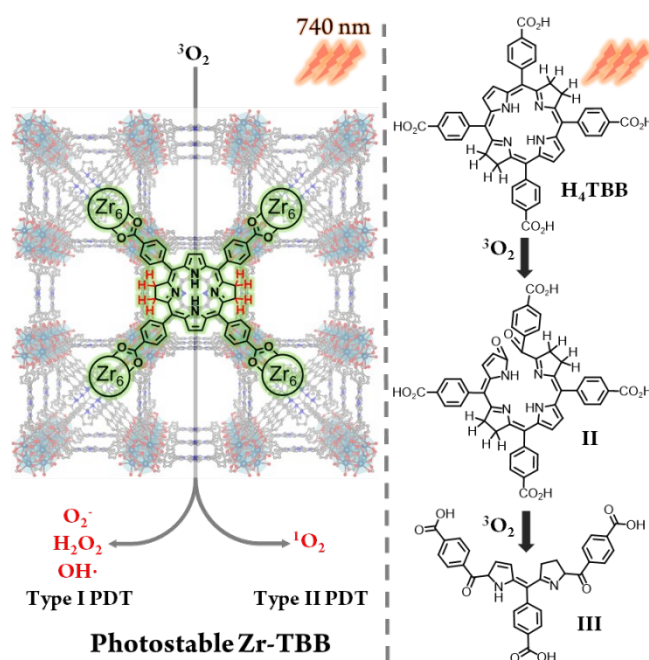
ABSTRACT: Herein we report the design of a bacteriochlorin-based nanoscale metal-organic framework, Zr-TBB, for highly effective photodynamic therapy via both type I and type II mechanisms. The framework of Zr-TBB stabilizes 5,10,15,20-tetra(*p*-benzoato)bacteriochlorin (TBB) ligands toward oxygen and light via geometrical constraint. Upon 740 nm light irradiation, Zr-TBB efficiently generates various reactive oxygen species, including singlet oxygen, superoxide anion, hydrogen peroxide and hydroxyl radicals to afford superb antitumor efficacy on mouse models of breast and colon cancers with cure rates of 40% and 60%, respectively.

Photodynamic therapy (PDT) is a minimally invasive and effective local therapy for many cancers,¹⁻⁵ but its clinical utility is limited by side effects from photosensitivity caused by residual photosensitizers (PSs) in normal tissues, shallow light penetration depth in tumors, and low oxygen concentrations in hypoxic tumors.⁶⁻⁸ As highly reduced derivatives of porphyrins and chlorins, bacteriochlorins possess several distinct features to overcome the challenges faced by conventional PSs: 1) weak absorption in the visible spectrum minimizes photosensitivity from ambient light, 2) strong absorption in the near-infrared region (700-850 nm) increases PDT efficacy, and 3) type I PDT tolerates hypoxia.⁹⁻¹¹ Padeliporfin, a Pd-coordinated bacteriochlorin, was approved in Europe for PDT treatment of prostate cancer.¹² However, bacteriochlorins are unstable toward oxygen and light,¹³⁻¹⁵ significantly reducing their potency in PDT.¹⁶⁻¹⁸

With tunable and porous structures,¹⁹⁻²² high PS loading,²³ and rigid structures,²⁴ nanoscale metal-organic frameworks (nMOFs) have emerged as novel nanophotosensitizers for PDT.²⁵⁻²⁸ By incorporating different PS ligands, nMOFs can be fine-tuned to optimize PDT efficacy. The rigid frameworks of nMOFs not only constrain the ligands from structural changes to reduce unimolecular photodecomposition but also isolate the PSs from each other to prevent inter-PS self-quenching.

Herein we report the use of nMOFs to stabilize bacteriochlorins for effective PDT. Experimental and computational studies demonstrated the stabilization of 5,10,15,20-tetra(*p*-benzoato)bacteriochlorin (TBB) ligands in the Zr-TBB nMOF toward oxygen and light owing to geometrical constraint by the framework. Zr-TBB mediated effective PDT via both type I and type II mechanisms by generating various reactive oxygen species (ROSs), including superoxide anion ($O_2^{\cdot-}$), hydrogen peroxide

(H_2O_2), hydroxyl radicals ($\cdot OH$), and singlet oxygen (1O_2), upon irradiation at 740 nm (Scheme 1). Zr-TBB showed superb *in vivo* antitumor efficacy on 4T1 and MC38 bearing mouse models of breast and colon cancers to afford cure rates of 40% and 60%, respectively.



Scheme 1. Stabilization of bacteriochlorin ligands in Zr-TBB for type I and type II PDT.

The new bacteriochlorin H₄TBB was synthesized via solvent-free reduction of 5,10,15,20-tetra(*p*-benzoato)porphyrin (H₄TBP) with *p*-toluenesulfonyl hydrazide (Figure S1).²⁹ The UV-vis spectrum of H₄TBB in *N,N*-dimethylformamide (DMF) exhibited four major peaks (Figure 1e) assignable to the transitions from two HOMOs (HOMO-1 and HOMO) to two LUMOs (LUMO and LUMO+1) based on four-orbital model.³⁰ For H₄TBB, the B_y peak at $\lambda_{max} = 361$ nm had a molar extinction coefficient (ϵ) of $70.4 \text{ mM}^{-1} \cdot \text{cm}^{-1}$ whereas the B_x peak at $\lambda_{max} = 377$ nm had an ϵ of $73.4 \text{ mM}^{-1} \cdot \text{cm}^{-1}$. These ϵ values are ~ 4 times lower than those of Soret bands in H₄TBP ($\epsilon_{420} = 460 \text{ mM}^{-1} \cdot \text{cm}^{-1}$) and 5,10,15,20-tetra(*p*-benzoato)chlorin (H₄TBC, $\epsilon_{420} = 381 \text{ mM}^{-1} \cdot \text{cm}^{-1}$), suggesting that

H₄TBB might alleviate photosensitivity side effects from ambient light.²⁶ The Q_x and Q_y peaks of H₄TBB had an ϵ_{521} of 32.4 mM⁻¹·cm⁻¹ and an ϵ_{742} of 58.4 mM⁻¹·cm⁻¹, respectively. The Q_y peak of H₄TBB at 742 nm is nearly ideal for tissue penetration, and H₄TBB has ~12 and ~2 times higher ϵ values than those of H₄TBP and H₄TBC, respectively.²⁶ H₄TBB is thus a superior PS over H₄TBP and H₄TBC with an optimal Q_y wavelength and a much higher ϵ .³¹

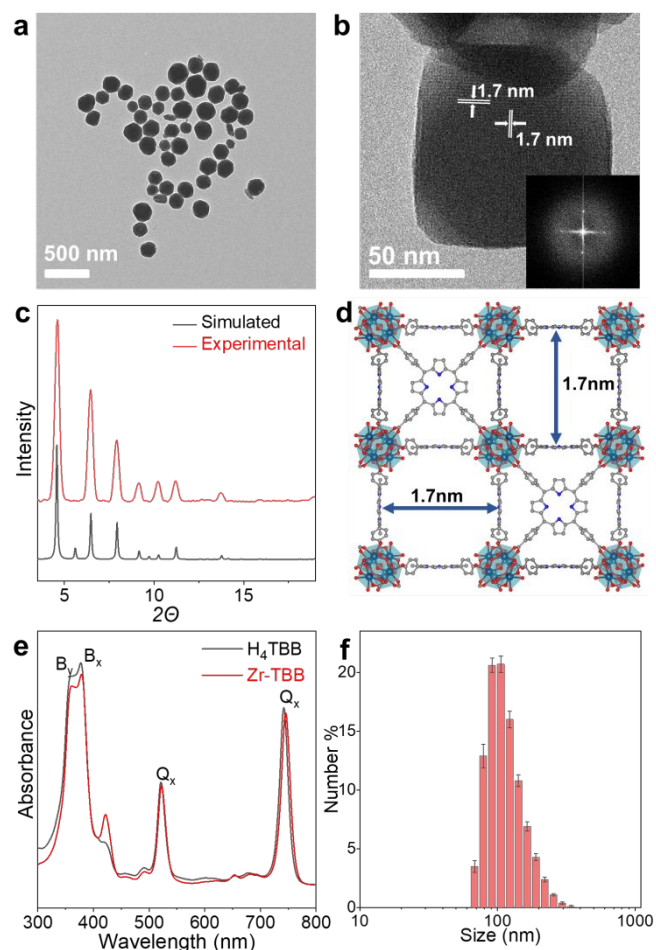


Figure 1. TEM image (a), HR-TEM image and FFT pattern (inset) (b), PXRD pattern (c), X-ray crystal structure (d), UV-vis spectra in DMF (e), and DLS number-averaged diameter in EtOH (f) of Zr-TBB.

Zr-TBB was synthesized via a solvothermal reaction of ZrCl₄, H₄TBB, and 88% formic acid in DMF at 100 °C under anaerobic conditions. Single crystal X-ray diffraction of Hf-TBB revealed a PCN-224 structure in the *Im* $\bar{3}$ m space group with Hf₆(μ_3 -O)₄(μ_3 -OH)₄ SBUs linked by TBB ligands to afford a 3-D framework of *shc* topology (Figure 1d and Figure S3).³² Powder X-ray diffraction pattern (PXRD) studies indicated that Zr-TBB adopted the same structure as Hf-TBB (Figure 1c) with a formula of [Zr₆(μ_3 -O)₄(μ_3 -OH)₄(OH)₆(H₂O)₆]₂(TBB)₃. Inductively coupled plasma-mass spectrometry (ICP-MS) and UV-vis spectra gave a Zr to TBB ratio of 4.22, which is slightly lower than the theoretical ratio of 4 likely due to minor decomposition of TBB ligands during nMOF synthesis. Thermogravimetric analysis showed a weight loss of 65.9% in the 25 - 600 °C range, consistent to the expected value of 64.3% for the conversion of Zr-TBB to ZrO₂ (Figure S6).

Dynamic light scattering (DLS) of Zr-TBB revealed a number-averaged size of 117.9 ± 1.4 nm, with a polydispersity index of

0.09 (Figure 1f). Transmission electron microscopy (TEM) imaging (Figure 1a, 1b, S4, S5) revealed spherical to cubic morphology for Zr-TBB with a diameter of approximately 100 nm. High resolution TEM (HR-TEM) imaging gave a lattice spacing of 1.7 nm (Figure 1b) for Zr-TBB while the fast Fourier transform (FFT) patterns (Figure 1b inset) revealed the tetragonal symmetry, consistent with projection down to the crystallographic axis (Figure 1d). Additionally, the UV-vis spectrum of Zr-TBB showed the same number of peaks as H₄TBB, with the appearance of a small TBC Soret peak at ~422 nm due to slight oxidation of TBB (4%) during nMOF synthesis.

Photostability of H₄TBB and Zr-TBB was tested in air-saturated DMF at a 5 μ M TBB concentration at 740 nm (100 mW·cm⁻²). After irradiation for 5 minutes, the Q_y peak absorbance of H₄TBB dropped to <4% of the original value, indicating its severe photobleaching (Figure 2a). In contrast, Zr-TBB retained 73% and 65% of the Q_y peak absorbance after light irradiation for 15 and 30 minutes, respectively, indicating its much enhanced photostability over H₄TBB. The photodecomposition quantum yield of Zr-TBB ($\Phi_{pd} = 8.14 \times 10^{-4}$) was 14 times lower than that of H₄TBB ($\Phi_{pd} = 1.15 \times 10^{-2}$, Table S2). The improved TBB stability of Zr-TBB can be attributed to the spatial constraint of the nMOF framework which prevents TBB from undergoing structural changes before photooxidation can occur and the site isolation effect of Zr-TBB which prevents TBB ligands from biomolecular decomposition.³³ We found photostability of Zr-TBB and H₄TBB was much improved in oxygen-free condition (Figure S7).

We used high resolution mass spectrometry (HR-MS) to characterize the photobleaching products of Zr-TBB and H₄TBB after 740 nm irradiation (100 mW·cm⁻²) in air-saturated DMF for 4 h. Photo-irradiated Zr-TBB was digested with 10% H₃PO₄ in DMSO before HR-MS analysis. For H₄TBB, the [H₄TBB+H⁺] peak at m/z=795.2 disappeared with the appearance of [M+H⁺] at 563.5 assignable to (Z)-4-(2-((4-carboxy-benzoyl)-1H-pyrrol-2-yl)(4-carboxy-phenyl)methylene)-3,4-dihydro-2H-pyrrole-5-carbonyl)benzoic acid (**III**, Scheme 1), a known fragmentation product from bacteriochlorin photobleaching.³⁴ The fragmentation of H₄TBB during photooxidation was supported by the UV-vis spectrum which showed two new peaks at 327 nm and 406 nm for **III** and disappearance of all peaks corresponding to H₄TBB (Figure S7e). In contrast, only H₄TBC at m/z=793.3 ([M+H⁺]) was recovered from the digested photo-irradiated Zr-TBB with no evidence of known photo-fragments. TBC can be generated by direct oxidation the pyrroline ring of TBB without significant structural change on the bacteriochlorin.

UV-vis spectroscopy was used to quantify photobleaching products of H₄TBB (Figure 2c) and Zr-TBB (Figure 2d) after light irradiation for 1-30 minutes (Figure S7a, S7b). H₄TBB was nearly completely photobleached (95%) within 5 minutes to generate mostly fragmentation product **III** (95%) and a negligible amount of H₄TBC (<0.1%). In contrast, Zr-TBB retained 84% TBB in 5 minutes with the formation of 4% TBC. Only 12% of TBB decomposed into unknown photoproducts. As TBC is also a good PS, TBB retained 80% and 74% PDT efficacy after light irradiation for 15 and 30 minutes, respectively. The photostability of Zr-TBB was supported by the maintenance of crystallinity as determined by PXRD (Figure 2b).

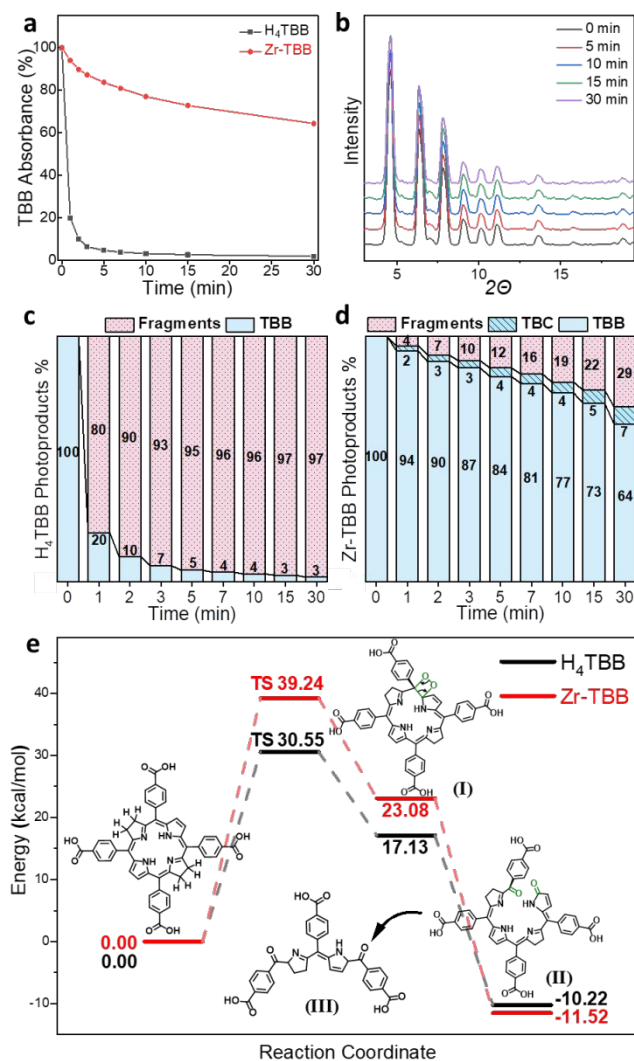


Figure 2. (a) Time-dependent TBB UV-vis absorbance after light irradiation in air-saturated DMF. (b) Time-dependent PXRD patterns of Zr-TBB after light irradiation. Percentages of photoproducts (TBB, TBC, fragments) of H₄TBB (c) and Zr-TBB (d) throughout 30-minute light irradiation. (e) Energy profiles of TBB photo-fragmentation in H₄TBB and Zr-TBB calculated by DFT.

Photobleaching of bacteriochlorins typically starts with [2+2] peroxidation reaction between C=C double bonds and O₂ (Figure 2e).³⁵ The peroxidized intermediate **I** breaks the π -conjugated bacteriochlorin ring and converts sp²-carbons into sp³-carbons, leading to significant distortion from the planar structure of TBB. The peroxide bridge is cleaved into two ketones in intermediate **II** via retro-[2+2] cyclization. Successive peroxidation and retro-[2+2] cyclization form fragmentation product **III**. However, the rigid framework of Zr-TBB prohibits TBB ligands from undergoing large structural changes, shutting down light-mediated peroxidation pathway. The pyrrole rings of the bacteriochlorin can still be oxidized to form TBC ligands without disturbing π -conjugation.

Density functional theory (DFT) calculations were performed to support the photostability difference of bacteriochlorins in H₄TBB and Zr-TBB (Figure 2e). The crystal structure of Zr-TBB was used and the structures of the carboxylate groups were frozen during DFT optimization to mimic spatial constraints in the nMOF. In the calculated energy profiles, H₄TBB displayed a ΔG^\ddagger of 30.6

kcal/mol (1.33 eV) while the constrained TBB in Zr-TBB exhibited a much higher ΔG^\ddagger of 39.2 kcal/mol (1.70 eV). The 1.69 eV energy in the 740 nm light source was thus sufficient to overcome the ΔG^\ddagger in H₄TBB but insufficient to overcome the ΔG^\ddagger in Zr-TBB, which explained the resistance of Zr-TBB to peroxidation and photo-fragmentation.

Bacteriochlorins can generate multiple ROSs via both type I (O₂^{•-}, H₂O₂, and \cdot OH) and type II (¹O₂) mechanisms.³⁶ The generation of O₂^{•-}, H₂O₂, \cdot OH, and ¹O₂ by H₄TBB and Zr-TBB was confirmed by electron paramagnetic resonance, hydrogen peroxide detection kit, aminophenyl fluorescein assay (APF), and singlet oxygen sensor green assay (SOSG), respectively. Due to photobleaching, H₄TBB showed much weaker signals of type I ROSs than Zr-TBB (Figure S12-S14). Similarly, ¹O₂ generation of H₄TBB reached plateau within 1 minute of light irradiation while Zr-TBB showed a linear increase of ¹O₂ signal throughout the 15-minute experiment (Figure S15).

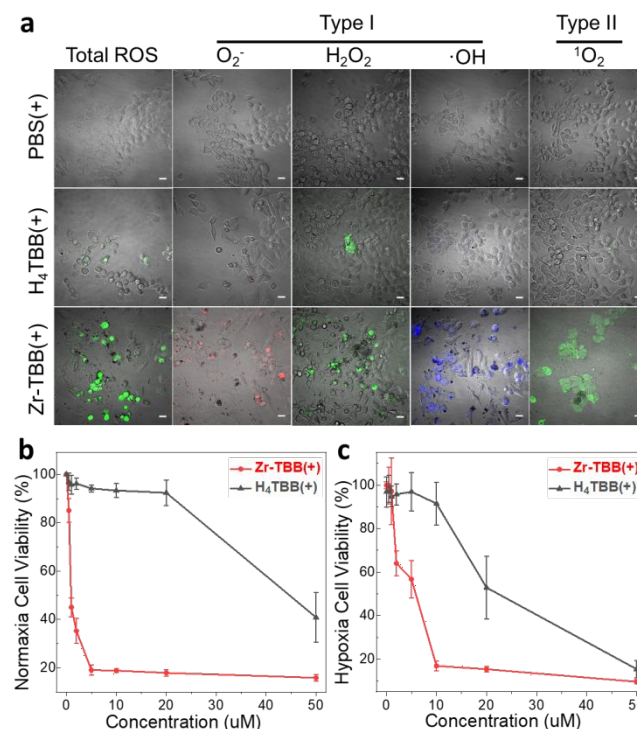


Figure 3. (a) CLSM images of various ROS species generated in 4T1 cells after light irradiation. Total ROS was detected by H2DCFDA assay. Scale bar is 20 μ m. (b,c) MTS assays of Zr-TBB(+) and H₄TBB(+) under normoxic (b) and hypoxic (c) conditions.

We next examined cellular uptake, *in vitro* ROS generation, and cytotoxicity of H₄TBB and Zr-TBB on 4T1 murine breast carcinoma cells. ICP-MS and UV-vis studies showed that 4T1 cells uptook significantly more Zr-TBB than H₄TBB (Figure S17). The *in vitro* generation of O₂^{•-}, H₂O₂, \cdot OH and ¹O₂ by Zr-TBB plus light irradiation [denoted Zr-TBB(+)] was detected under confocal laser scanning microscopy (CLSM) with superoxide detection, intracellular hydrogen peroxide, coumarin-3-carboxylic acid assay and SOSG assay kits, respectively (Figure 3a). The generation of ¹O₂ and O₂^{•-} by Zr-TBB(+) was confirmed by flow cytometric analyses. H₄TBB(+) generated much less ROSs than Zr-TBB(+), likely due to low cellular uptake, oxidation, and photobleaching. Zr-TBB(+) efficiently generated four different kinds of ROSs to facilitate type I and type II PDT. The cytotoxicity of Zr-TBB(+) was determined by MTS assay. Under normoxic condition, Zr-TBB(+) exhibited an IC₅₀ of 0.91 \pm 0.77 μ M on 4T1 cells while

H₄TBB(+) did not show any cytotoxicity at ≤ 20 μ M (Figure 3b). Under hypoxic condition, the IC₅₀ values of Zr-TBB(+) and H₄TBB(+) on 4T1 cells were 2.94 ± 0.76 μ M and 19.50 ± 0.82 μ M, respectively (Figure 3c). The increased cytotoxicity of H₄TBB(+) under hypoxia likely resulted from reduced photobleaching at low O₂ concentration. The apoptosis of 4T1 cells after PDT treatments were evaluated by flow cytometry with Annexin-V and propidium iodide staining. Zr-TBB(+) treated cells gave significantly stronger apoptosis signals than those treated with H₄TBB(+) and PBS(+) (Figure S19). Flow cytometry and CLSM imaging studies also showed that Zr-TBB(+) treated cells exhibited much stronger calreticulin (CRT) signals than those treated with H₄TBB(+) and PBS(+) (Figure S23-24), indicating more pronounced immunogenic cell death (ICD) caused by Zr-TBB(+).

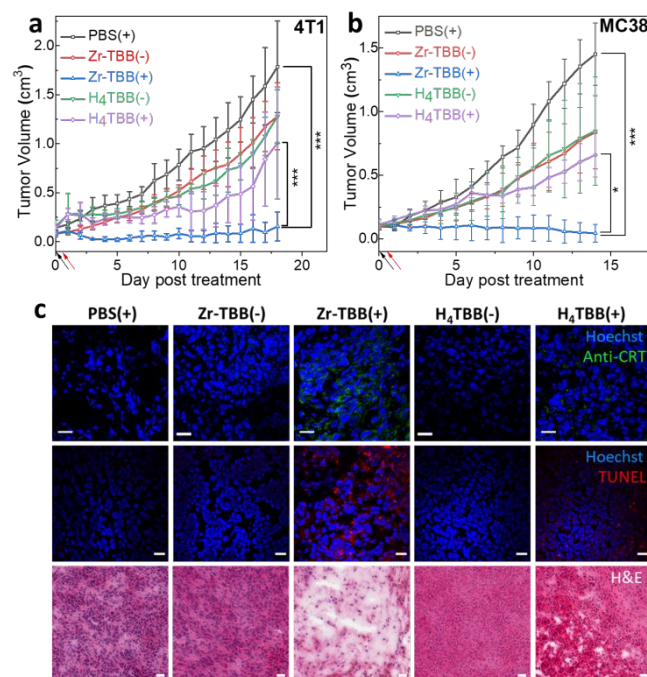


Figure 4. Antitumor efficacy on 4T1 bearing BALB/c mice (a) and MC38 bearing C57Bl/6 mice (b). (c) CLSM imaging of cell surface CRT (top) and cell apoptosis (middle) and H&E staining showing severe apoptosis and necrosis (bottom) after Zr-TBB(+) treatment on 4T1 tumors. Scale bar is 20 μ m.

The *in vivo* anti-tumor efficacy was investigated on subcutaneous 4T1 bearing BALB/c mice and murine colon carcinoma MC38 bearing C57Bl/6 mice. Zr-TBB(+) exhibited excellent therapeutic effects to afford 91% tumor growth inhibition and a 40% cure rate on 4T1 model (Figure 4a) and 97% tumor growth inhibition and a 60% cure rate on MC38 model. H&E staining showed severe necrosis in Zr-TBB(+) treated 4T1 tumors. TUNEL (Figure 4c) and CRT expression (Figure 4d) assays by CLSM showed strong apoptosis and ICD induced by Zr-TBB(+) treatment. Finally, steady body weight and minimal abnormalities of major organ sections indicated that Zr-TBB had no systematic toxicity on BALB/c and C57Bl/6 mice.

In summary, we report the use of the framework of Zr-TBB nMOF to stabilize bacteriochlorins toward oxygen and light irradiation. Zr-TBB mediated effective PDT by generating O₂⁻, H₂O₂, \cdot OH, and ¹O₂ via both type I and type II mechanisms. Zr-TBB showed superb *in vivo* antitumor efficacy on mouse tumor models of breast and colon cancers to afford cure rates of 40% and 60%, respectively. nMOFs thus present a unique platform to design novel nanophotosensitizers based on bacteriochlorins and other unstable photosensitizing molecules.

ASSOCIATED CONTENT

Supporting Information

The Supporting Information is available free of charge on the ACS Publications website.

Data for Hf-TBB single crystal (CIF)

Synthesis and characterization of H₄TBB and Zr-TBB, ROS generation and mechanism, anticancer efficacy, and DFT calculation (PDF)

AUTHOR INFORMATION

Corresponding Author

*wenbinlin@uchicago.edu

ORCID

Taokun Luo: 0000-0001-5894-0490

Kaiyuan Ni: 0000-0002-8152-6746

Guangxu Lan: 0000-0002-0415-5849

Wenbin Lin: 0000-0001-7035-7759

Author Contributions

*T.L. and *K.N. contributed equally.

Notes

The authors declare no competing financial interest.

ACKNOWLEDGMENT

We thank Yang Song, Xuanyu Feng, Yunhong Pi, and Wenbo Han for experimental help. We acknowledge the National Cancer Institute (U01-CA198989) and the University of Chicago Medicine Comprehensive Cancer Center (NIH CCSG: P30 CA014599) for funding support. NSF's ChemMatCARS Sector 15 is principally supported by the Divisions of Chemistry (CHE) and Materials Research (DMR), National Science Foundation, under Grant NSF/CHE-1834750. Use of the Advanced Photon Source, an Office of Science User Facility operated for the U.S. Department of Energy (DOE) Office of Science by Argonne National Laboratory, was supported by the U.S. DOE under Contract DE-AC02-06CH11357.

REFERENCES

1. Lovell, J. F.; Liu, T. W.; Chen, J.; Zheng, G., Activatable photosensitizers for imaging and therapy. *Chem. Rev.* **2010**, *110* (5), 2839-2857.
2. Luby, B. M.; Walsh, C. D.; Zheng, G., Advanced photosensitizer activation strategies for smarter photodynamic therapy beacons. *Angew. Chem. Int. Ed.* **2019**, *58* (9), 2558-2569.
3. Huang, H.-C.; Mallidi, S.; Liu, J.; Chiang, C.-T.; Mai, Z.; Goldschmidt, R.; Ebrahim-Zadeh, N.; Rizvi, I.; Hasan, T., Photodynamic therapy synergizes with irinotecan to overcome compensatory mechanisms and improve treatment outcomes in pancreatic cancer. *Cancer Res.* **2016**, *76* (5), 1066-1077.
4. Dolmans, D. E.; Fukumura, D.; Jain, R. K., Photodynamic therapy for cancer. *Nat. Rev. Cancer.* **2003**, *3* (5), 380-387.
5. Shao, S.; Rajendiran, V.; Lovell, J. F., Metalloporphyrin nanoparticles: Coordinating diverse theranostic functions. *Coord. Chem. Rev.* **2019**, *379*, 99-120.
6. Lan, G.; Ni, K.; Xu, Z.; Veroneau, S. S.; Song, Y.; Lin, W., Nanoscale metal-organic framework overcomes hypoxia for

- photodynamic therapy primed cancer immunotherapy. *J. Am. Chem. Soc.* **2018**, *140* (17), 5670-5673.
7. Hopper, C., Photodynamic therapy: a clinical reality in the treatment of cancer. *Lancet. Oncol.* **2000**, *1* (4), 212-219.
8. Mallidi, S.; Anbil, S.; Bulin, A.-L.; Obaid, G.; Ichikawa, M.; Hasan, T., Beyond the barriers of light penetration: strategies, perspectives and possibilities for photodynamic therapy. *Theranostics* **2016**, *6* (13), 2458.
9. Chen, Y.; Li, G.; Pandey, R. K., Synthesis of bacteriochlorins and their potential utility in photodynamic therapy (PDT). *Curr. Org. Chem.* **2004**, *8* (12), 1105-1134.
10. Zhou, Z.; Song, J.; Nie, L.; Chen, X., Reactive oxygen species generating systems meeting challenges of photodynamic cancer therapy. *Chem. Soc. Rev.* **2016**, *45* (23), 6597-6626.
11. Lan, G.; Ni, K.; Veroneau, S. S.; Feng, X.; Nash, G. T.; Luo, T.; Xu, Z.; Lin, W., Titanium-Based Nanoscale Metal–Organic Framework for Type I Photodynamic Therapy. *J. Am. Chem. Soc.* **2019**, *141* (10), 4204-4208.
12. Azzouzi, A.-R.; Vincendeau, S.; Barret, E.; Cicco, A.; Kleinclauss, F.; van der Poel, H. G.; Stief, C. G.; Rassweiler, J.; Salomon, G.; Solsona, E.; Alcaraz, A.; Tammela, T. T.; Rosario, D. J.; Gomez-Veiga, F.; Ahlgren, G.; Benzaghoul, F.; Gaillac, B.; Amzal, B.; Debruyne, F. M. J.; Fromont, G.; Gratzke, C.; Emberton, M., Padeliporfin vascular-targeted photodynamic therapy versus active surveillance in men with low-risk prostate cancer (CLIN1001 PCM301): an open-label, phase 3, randomised controlled trial. *Lancet. Oncol.* **2017**, *18* (2), 181-191.
13. Pucelik, B.; Arnaut, L. G.; Stochel, G.; Dąbrowski, J. M., Design of Pluronic-Based Formulation for Enhanced Redaporfin-Photodynamic Therapy against Pigmented Melanoma. *ACS Appl. Mater. Interfaces* **2016**, *8* (34), 22039-22055.
14. Huang, Y. Y.; Balasubramanian, T.; Yang, E.; Luo, D.; Diers, J. R.; Bocian, D. F.; Lindsey, J. S.; Holten, D.; Hamblin, M. R., Stable synthetic bacteriochlorins for photodynamic therapy: role of dicyano peripheral groups, central metal substitution (2H, Zn, Pd), and Cremophor EL delivery. *Chem. Med. Chem.* **2012**, *7* (12), 2155-2167.
15. Dąbrowski, J. M.; Arnaut, L. G., Photodynamic therapy (PDT) of cancer: from local to systemic treatment. *Photochemical & Photobiological Sciences* **2015**, *14* (10), 1765-1780.
16. Grahm, M. F.; McGuinness, A.; Benzie, R.; Boyle, R.; de Jode, M. L.; Dilkes, M. G.; Abbas, B.; Williams, N. S., Intracellular uptake, absorption spectrum and stability of the bacteriochlorin photosensitizer 5, 10, 15, 20-tetrakis (m-hydroxyphenyl) bacteriochlorin (mTHPBC). Comparison with 5, 10, 15, 20-tetrakis (m-hydroxyphenyl) chlorin (mTHPC). *J. Photochem. Photobiol. B: Biol.* **1997**, *37* (3), 261-266.
17. Huang, L.; Huang, Y.-Y.; Mroz, P.; Tegos, G. P.; Zhiyentayev, T.; Sharma, S. K.; Lu, Z.; Balasubramanian, T.; Kraymer, M.; Ruzi, C., Stable synthetic cationic bacteriochlorins as selective antimicrobial photosensitizers. *Antimicrob. Agents Chemother.* **2010**, *54* (9), 3834-3841.
18. Pandey, R. K.; Constantine, S.; Tsuchida, T.; Zheng, G.; Medforth, C. J.; Aoudia, M.; Kozyrev, A. N.; Rodgers, M. A.; Kato, H.; Smith, K. M., Synthesis, photophysical properties, *in vivo* photosensitizing efficacy, and human serum albumin binding properties of some novel bacteriochlorins. *J. Med. Chem.* **1997**, *40* (17), 2770-2779.
19. Furukawa, H.; Cordova, K. E.; O’Keeffe, M.; Yaghi, O. M., The chemistry and applications of metal-organic frameworks. *Science* **2013**, *341* (6149), 1230444.
20. Chen, B.; Xiang, S.; Qian, G., Metal–organic frameworks with functional pores for recognition of small molecules. *Acc. Chem. Res.* **2010**, *43* (8), 1115-1124.
21. Long, J. R.; Yaghi, O. M., The pervasive chemistry of metal–organic frameworks. *Chem. Soc. Rev.* **2009**, *38* (5), 1213-1214.
22. Liu, C.; Zeng, C.; Luo, T.-Y.; Merg, A. D.; Jin, R.; Rosi, N. L., Establishing porosity gradients within metal–organic frameworks using partial postsynthetic ligand exchange. *J. Am. Chem. Soc.* **2016**, *138* (37), 12045-12048.
23. Fateeva, A.; Chater, P. A.; Ireland, C. P.; Tahir, A. A.; Khimiyak, Y. Z.; Wiper, P. V.; Darwent, J. R.; Rosseinsky, M. J., A Water - Stable Porphyrin - Based Metal - Organic Framework Active for Visible - Light Photocatalysis. *Angew. Chem.* **2012**, *124* (30), 7558-7562.
24. Shustova, N. B.; Cozzolino, A. F.; Dincă, M., Conformational locking by design: Relating strain energy with luminescence and stability in rigid metal–organic frameworks. *J. Am. Chem. Soc.* **2012**, *134* (48), 19596-19599.
25. Lan, G.; Ni, K.; Lin, W., Nanoscale metal–organic frameworks for phototherapy of cancer. *Coord. Chem. Rev.* **2019**, *379*, 65-81.
26. Lu, K.; He, C.; Guo, N.; Chan, C.; Ni, K.; Weichselbaum, R. R.; Lin, W., Chlorin-based nanoscale metal–organic framework systemically rejects colorectal cancers via synergistic photodynamic therapy and checkpoint blockade immunotherapy. *J. Am. Chem. Soc.* **2016**, *138* (38), 12502-12510.
27. Ni, K.; Aung, T.; Li, S.; Fatuzzo, N.; Liang, X.; Lin, W., Nanoscale metal-Organic framework mediates radical therapy to enhance cancer immunotherapy. *Chem* **2019**, *5* (7), 1892-1913.
28. Ni, K.; Luo, T.; Lan, G.; Culbert, A.; Song, Y.; Wu, T.; Jiang, X.; Lin, W., A Nanoscale Metal–Organic Framework to Mediate Photodynamic Therapy and Deliver CpG Oligodeoxynucleotides to Enhance Antigen Presentation and Cancer Immunotherapy. *Angew. Chem.* **2020**, *132* (3), 1124-1128.
29. Pereira, M. M.; Monteiro, C. J. P.; Simões, A. V. C.; Pinto, S. M. A.; Abreu, A. R.; Sá, G. F. F.; Silva, E. F. F.; Rocha, L. B.; Dąbrowski, J. M.; Formosinho, S. J.; Simões, S.; Arnaut, L. G., Synthesis and photophysical characterization of a library of photostable halogenated bacteriochlorins: an access to near infrared chemistry. *Tetrahedron* **2010**, *66* (49), 9545-9551.
30. Ghosh, A., Theoretical Comparative Study of Free Base Porphyrin, Chlorin, Bacteriochlorin, and Isobacteriochlorin: Evaluation of the Potential Roles of ab Initio Hartree–Fock and Density Functional Theories in Hydroporphyrin Chemistry. *J. Phys. Chem. B* **1997**, *101* (16), 3290-3297.
31. Bashkatov, A. N.; Berezin, K. V.; Dvoretzkiy, K. N.; Chernavina, M. L.; Genina, E. A.; Genin, V. D.; Kochubey, V. I.; Lazareva, E. N.; Pravdin, A. B.; Shvachkina, M. E., Measurement of tissue optical properties in the context of tissue optical clearing. *J. Biomed. Opt.* **2018**, *23* (9), 091416.
32. Feng, D.; Chung, W.-C.; Wei, Z.; Gu, Z.-Y.; Jiang, H.-L.; Chen, Y.-P.; Darensbourg, D. J.; Zhou, H.-C., Construction of ultrastable porphyrin Zr metal–organic frameworks through linker elimination. *J. Am. Chem. Soc.* **2013**, *135* (45), 17105-17110.
33. Strattonnikov, A. A.; Meerovich, G. A.; Loschenov, V. B. In *Photobleaching of photosensitizers applied for photodynamic therapy*, Optical Methods for Tumor Treatment and Detection: Mechanisms and Techniques in Photodynamic Therapy IX, International Society for Optics and Photonics: 2000; pp 81-91.
34. Bonnett, R.; Martinez, G., Photobleaching of compounds of the 5, 10, 15, 20-Tetrakis (m-hydroxyphenyl) porphyrin Series (m-THPP, m-THPC, and m-THPBC). *Org. Lett.* **2002**, *4* (12), 2013-2016.
35. Bonnett, R.; Martinez, G., Photobleaching of sensitizers used in photodynamic therapy. *Tetrahedron* **2001**, *57* (47), 9513-9547.
36. Silva, E. F.; Serpa, C.; Dąbrowski, J. M.; Monteiro, C. J.; Formosinho, S. J.; Stochel, G.; Urbanska, K.; Simões, S.; Pereira, M. M.; Arnaut, L. G., Mechanisms of singlet - oxygen and superoxide - ion generation by porphyrins and bacteriochlorins and their implications in photodynamic therapy. *Chem. Eur* **2010**, *16* (30), 9273-9286.

Table of contents (8.25cm x 4.45cm)

